Roads to improve the performance of hybrid thermosolar gas turbine power plants: working fluids and multi-stage configurations

M.J. Santos, C. Miguel-Barbero, R.P. Merchán, A. Medina, A. Calvo Hernández

Department of Applied Physics, University of Salamanca, 37008 Salamanca, Spain

Abstract

This paper presents a general thermodynamic model for hybrid Brayton central tower thermosolar plants. These plants have been proved to be technically feasible but R+D efforts need to be done in order to improve its commercial interest. From the thermodynamic viewpoint it is necessary to increase its performance to get larger power production with reduced fuel consumption, and so reduced emissions. We develop a model for multi-step compression and expansion stages with that aim. The model is flexible and allows to simulate recuperative or non-recuperative plants, with an arbitrary number of stages and working with different subcritical fluids. The results for multi-step configurations are compared with those obtained for a plant with one turbine and one compressor. Different working fluids are analyzed, including air, nitrogen, carbon dioxide, and helium. Several plant layouts and the corresponding optimal pressure ratios are analyzed. It is concluded that configurations with two-stages compression with intercooling combined with one or two expansion stages can significantly improve overall plant efficiency and lower fuel consumption. Power block efficiencies can reach 0.50 and overall plant efficiency can attain values about 0.40 working with air or CO_2. For instance, comparing with a single stage plant running with air, a plant with subcritical CO_2, two compression stages with intercooling and single step expansion can reach an overall efficiency about 19% larger and a fuel conversion rate around 23% larger. For such configuration, the specific fuel consumption is predicted to be about 108 kg/(MW h) at design point conditions.

Keywords:

Email addresses: smjesus@usal.es (M.J. Santos), cesarmi@usal.es (C. Miguel-Barbero), rpmerchan@usal.es (R.P. Merchán), amd385@usal.es (A. Medina), anca@usal.es (A. Calvo Hernández)

Thermosolar hybrid power plants, Multi-stage Brayton cycle, Overall plant efficiency, Improved plant design
PACS: 05.70.Ln, 07.20.Pe, 84.60.-h

Nomenclature

A_a aperture area of the solar field

A_r solar receiver area

a_c isentropic compressor pressure ratio

a_t isentropic turbine pressure ratio

C solar collector concentration ratio

c_w specific heat of the working fluid

f solar share

G direct solar irradiance

h_1 radiation heat loss coefficient for the solar collector

h_2 effective convection and conduction loss coefficient for the solar collector

$\dot{m}$ mass flow rate of the working substance

$\dot{m}_f$ fuel mass flow rate in the main combustion chamber

$\dot{m}_{fi}$ fuel mass flow rate in reheaters

P power output

$|\dot{Q}_{\mathrm{C}}|$ heat losses at the combustion chamber

$|\dot{Q}_{\mathrm{H}}|$ total heat-transfer rate absorbed from the working fluid

$|\dot{Q}_{\mathrm{iHC}}|$ heat losses at the heat exchanger associated to the combustion chamber

$|\dot{Q}_{\mathrm{HC}}|$ heat rate input from the combustion chamber

$|\dot{Q}'_{\mathrm{HC}}|$ heat rate transferred from the combustion chamber to the associated heat exchanger

$|\dot{Q}_{\mathrm{HS}}|$ heat rate input from the solar collector

$|\dot{Q}_{\mathrm{iHS}}|$ heat losses at the solar receiver

$|\dot{Q}'_{\mathrm{HS}}|$ heat rate transferred from the solar collector to the associated heat exchanger

$|\dot{Q}_l|$ losses associated to heat transfers in the solar field

$|\dot{Q}_{\mathrm{L}}|$ heat-transfer rate between the working fluid and the ambient

Q_{LHV} lower heating value of the fuel

$|\dot{Q}_{reh}|$ heat rate input from the reheaters

r_e fuel conversion rate

r_p overall pressure ratio

T_{HC} working temperature of the combustion chamber

T_{HS} working temperature of the solar collector

T_{L} ambient temperature

T_x working fluid temperature after the heat input from the recuperator

$T_{x'}$ working fluid temperature after heat input from the solar collector

T_y working fluid exhaust temperature

T_1 compressors inlet temperature

T_2 temperature after last compressor

T_3 turbines inlet temperature

T_4 temperature after last turbine

U_{L} effective conduction-convection heat transfer coefficient

α effective emissivity

$\varepsilon_{\mathrm{HC}}$ combustion chamber heat exchanger effectiveness

$\varepsilon_{\mathrm{HS}}$ solar collector heat exchanger effectiveness

ε_L cold side heat exchanger effectiveness

ε_c isentropic efficiency of the compressors

ε_r recuperator effectiveness

ε_t isentropic efficiency of the turbines

γ adiabatic coefficient of the working fluid

η overall thermal efficiency

η_c combustion efficiency

η_h thermal efficiency of the Brayton heat engine

η_s solar collector efficiency

η_0 optical efficiency

ρ_{H} irreversibilities due to pressure drops in the heat input

ρ_L irreversibilities due to pressure drops in the heat release

σ Stefan-Boltzmann constant

1. Introduction

Concentrating solar power (CSP) is one of the promising renewable energy technologies that can contribute to decrease the dependence on fossil fuels for the generation of electricity and so, the environmental impact of energy production [1, 2, 3]. Unlike other renewable resources this technology is suited to produce non-intermittent power with the implementation of thermal storage or hybridization concepts [4, 5, 6]. We deal with the last, CSP plants that ensure an almost constant energy injection to the grid in the range of a few megawatts. These plants are not completely free of fossil fuel consumption and pollutant emissions because a backup combustion chamber ensures the power output to the grid but control is not complicated and energy release to the grid is predictable. For instance, the plants that work following a closed Brayton-like thermal cycle require a reduced water consumption compared with those working on Rankine cycles and can reach similar efficiencies [7]. This point is especially advantageous in arid regions with appropriate solar resources. To get those efficiencies quite high turbine inlet temperatures have to be reached in the solar receivers, about 800 - 1000 °C [8, 9, 10, 11]. Several experimental prototypes have shown that this is feasible using ceramic materials in central tower volumetric receivers or other alternatives. Pioneer demonstration size plants have arrived at the same conclusion: the technology is practicable but it is still necessary a R+D activity to look for ways to improve the overall plant efficiency in order to get commercially interesting levelized costs of electricity. Particularly, thermoeconomic studies show that there is still a wide margin for improvement in the power block [1].

Along this work line thermodynamic studies about possible refinements on the basic Brayton cycle and the effects of the working fluid are important to guide future plant designs. These studies allow to model the plant in terms of a reduced number of parameters and to predict realistic values for efficiencies or other output records [12, 13, 14, 15]. Thus, sensitivity studies and optimization analyses can be done in more general terms that those done, for instance, with simulation software [16, 17, 18, 19]. Both techniques are complementary. Probably, general thermodynamic models are to be developed first in order to select adequate plant concepts and then detailed component-to-component simulations are required to solve technical issues and to get to very detailed predictions of plant performance.

One of the main drawbacks to the consideration Brayton cycles in CSP ap-

plications is that for the compression stage much power is required, so the net power output becomes reduced. One possibility to avoid this handicap is to operate at supercritical conditions. Extensive work has been devoted to this issue, specially considering carbon dioxide as working fluid [12, 20, 21, 22]. Near the critical region fluids show numerical values for compressibility similar to liquids. Compression work can be reduced but high temperatures can be maintained. Nevertheless, as critical pressure for CO_2 is about 74 bar, high pressures have to be used which lead to several technical problems [23]. Moreover, wide fluctuations of thermodynamic properties near the critical point make difficult to develop thermodynamic models relying on ideal gas approximations. With respect to the turbomachinery much scarce experience has been acquired in components working with critical or transcritical fluids [24, 25, 20]. An alternative way to reduce compression work is by joining these concepts: recuperation and multi-stage compression with intercooling [1, 24, 26, 27]. Additionally, if expansion is performed in several turbines with intermediate reheaters, temperature at the exit of the last turbine is high and so the potential for recuperation.

Even though there is a great amount of works on the possibilities of the use of supercritical CO_2 in CSP systems [12, 24], to our knowledge there are much scarce thermodynamical investigations on subcritical fluids as CO_2 together with multi-stage compression with intercooling and multi-stage expansion with reheating. Our work deals with this point. We shall investigate plant configurations for central tower hybrid CSP plants working on closed atmospheric Brayton cycles for several working fluids, including subcritical CO_2, helium, nitrogen, and air. Plant performance will be compared by taking similar conditions for all fluids. Although the peculiarities of heat exchangers and turbomachinery of course rely on the type of fluid we shall assume components with similar effectivenesses or isentropic efficiencies, *i.e.*, we do not deal with details on the design and performance of plant components, but it is assumed that with the appropriate design particularities components can have similar effectivenesses or isentropic efficiencies. To get that aim we develop a thermodynamical model that incorporates the main irreversibilities existing in all the subsystems in these plants: solar, combustion chamber, and thermal engine. A simplified model was developed and validated in previous works by our group for the case of air and single-stage compression and expansion [28, 29, 30]. In this work it is extended for an arbitrary number of compression/expansion steps, recuperation, and for subcritical fluids by explicitly considering the temperature dependence of specific

heats. Although the model allows for on-design and off-design analyses, in this work we shall consider design point parameters from an experimental facility as reference case to compare with [11, 31]. The compression ratio is a key parameter in the design of any plant involving Brayton-like cycles. In our study, first the results for different fluids at the same compression ratio will be compared and later specific values of the pressure ratio for each working fluid leading to maximum overall plant efficiency will be calculated.

In Sec. 2 the thermodynamic model and the main hypotheses assumed will be detailed. Explicit equations for heat transfers, subsystem efficiencies, and overall thermal efficiency will be developed. Section 3 contains information about the considered reference plant, the design parameters, and the particularities of the elected working fluids. Numerical predictions on plant performance assuming the pressure ratio of the reference plant will be compared in Sec. 4 for different working gases. In Sec. 5 a numerical analysis to maximize plant performance in terms of the pressure ratio will be performed for each fluid. Section 6 is specifically devoted to plant configurations with two compression steps and intercooling. The plant performance for this kind of plant layouts will be compared for all the fluids considered.

2. Plant thermodynamics

The considered system is a gas-turbine power plant hybridized with a central tower solar concentration system. An sketch of the whole system is depicted in Fig. 1. Briefly, the working fluid enters the first compressor at a temperature T_1, and exits the last one (N_c) at a temperature T_2. Between each pair of compressors, an intercooler is considered with the aim that the inlet temperature at each compressor is always T_1. After the last compressor the heat input in the power unit is divided in three subsequent steps:

1. A recuperator is used to take advantage of the residual heat after the last turbine. The fluid temperature at the recuperator exit is denoted as T_x.

2. When solar conditions are adequate, the fluid is redirected through the the solar receiver and its temperature increases up to $T_{x'}$.

3. During night or poor insolation conditions the working fluid is conducted directly to the combustion subsystem. We are considering a closed cycle, so the heat input from combustion is done through a heat

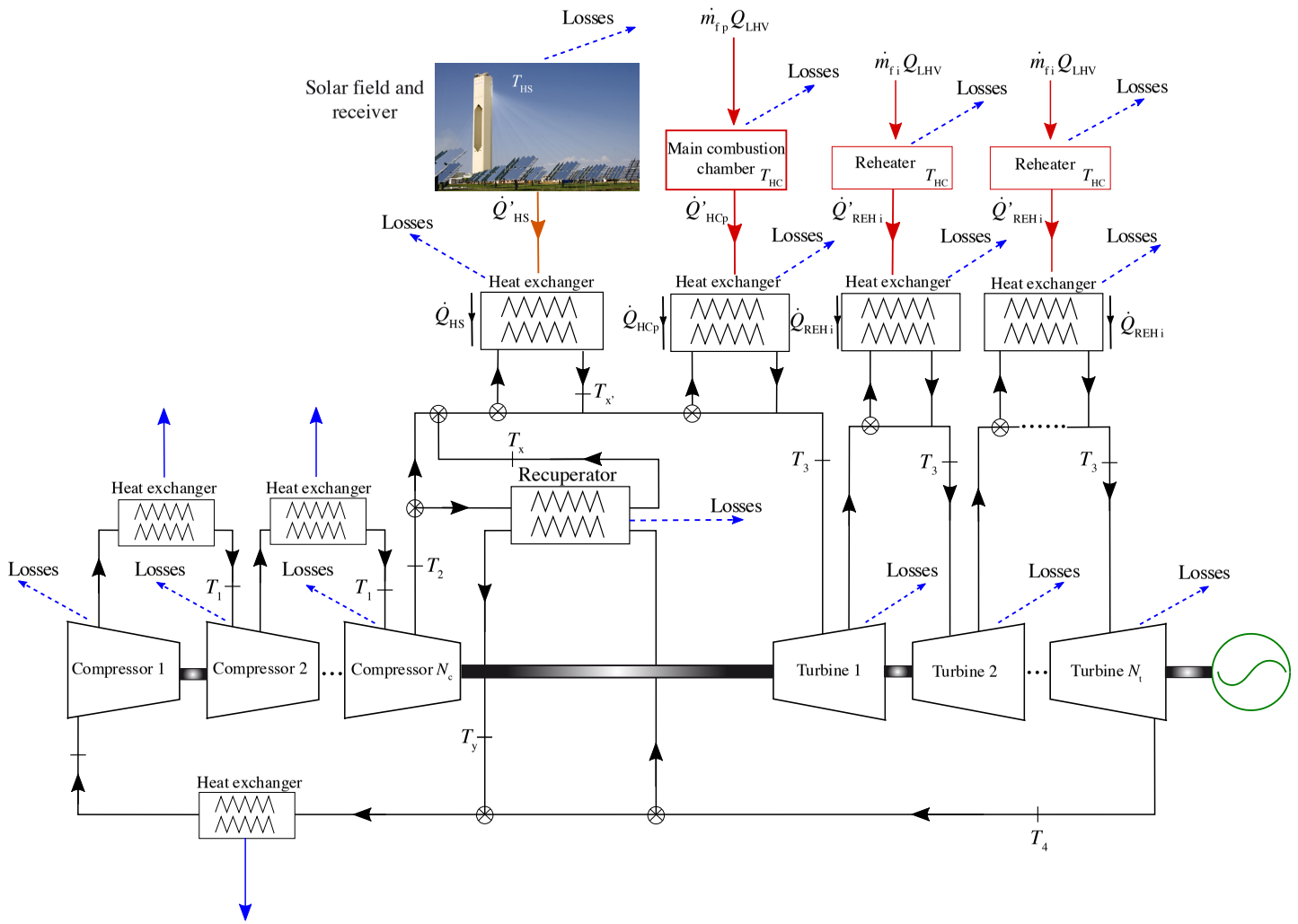

Figure 1: Scheme of the hybrid solar gas-turbine plant considered. The plant includes a solar subsystem (solar field and central tower receiver), a main combustion chamber, an arbitrary number of compressors (N_c), and an arbitrary number of turbines (N_t). Between compressors $N_c - 1$ intercoolers are considered and, similarly, between turbines $N_t - 1$ intermediate reheaters. Losses in the thermodynamic model are shown in the picture. The ambient temperature, T_L, and the effective temperature of the solar receiver, T_{HS}, are fluctuating quantities, since depend on seasonal and meteorological conditions.

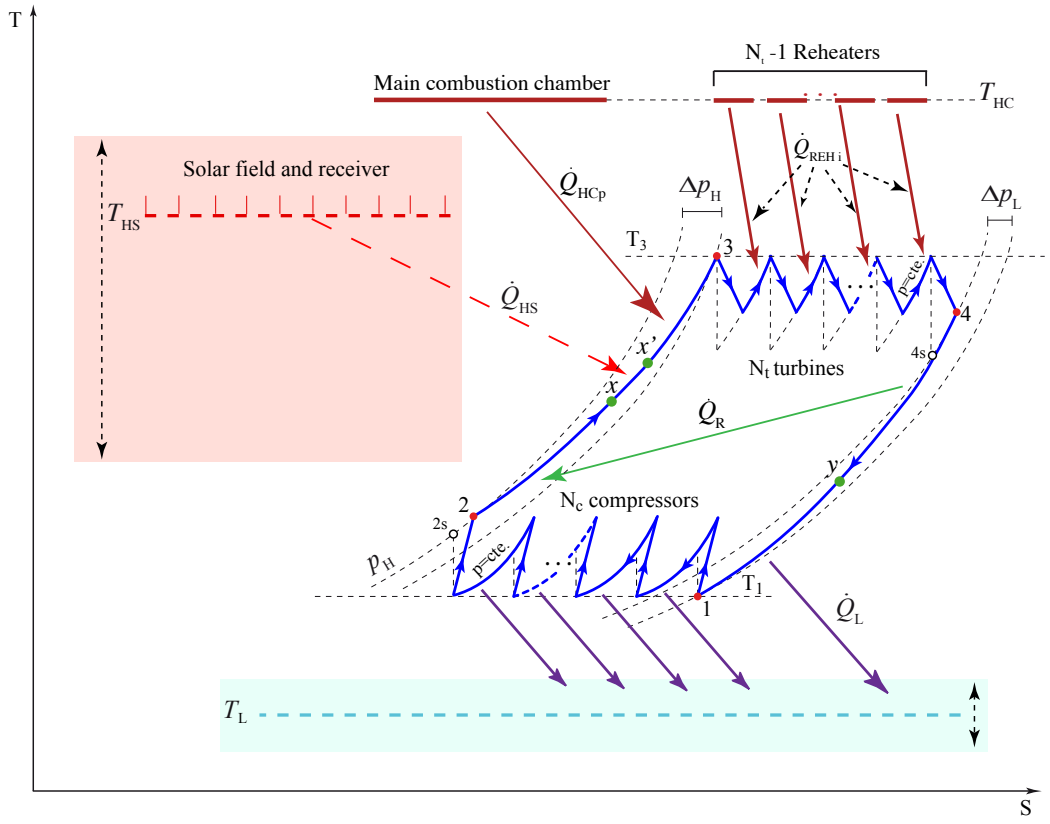

Figure 2: Temperature-entropy diagram of the considered plant layout.

exchanger associated to the main combustion chamber. Independently of solar conditions the combustion chamber ensures that the first turbine inlet temperature is stable, T_3.

The expansion stroke is performed by means of an arbitrary number of turbines, N_t. A number $N_t - 1$ of intermediate reheaters make that for any turbine the inlet temperature is T_3. Afterwards the expansion process (temperature T_4) the fluid is redirected through the recuperator to another heat exchanger that ensures that the process is closed and cyclic, so the temperature at the compressor entrance in the following cycle is T_1. Figure 2 contains a $T - S$ diagram of the thermodynamic cycle the plant follows.

2.1. Heat fluxes, subsystem efficiencies, and overall efficiency

The overall plant thermal efficiency, η, is defined as the fraction between the net mechanical power output, P, and the total heat input rate in the whole system. The latter is the sum of the heat input flows of the solar part and the combustion chamber:

$$\eta = \frac{P}{G\,A_a + \dot{m}_f\,Q_{\mathrm{LHV}}} \tag{1}$$

where G is the direct normal irradiance, A_a the aperture area of the heliostats field, Q_{LHV} the lower heating value of the fuel, and $\dot{m}_f$ is the sum of the fuel mass flows entering into the combustion chamber, $\dot{m}_{fp}$, as well as into the reheaters, $\dot{m}_{fi}$:

$$\dot{m}_f = \dot{m}_{fp} + \sum_{i=1}^{N_t-1} \dot{m}_{fi} \tag{2}$$

so, the overall efficiency is:

$$\eta = \frac{P}{G\,A_a + \left(\dot{m}_{fp} + \sum_{i=1}^{N_t-1} \dot{m}_{fi}\right) Q_{\mathrm{LHV}}} \tag{3}$$

Once expressed the efficiency in general terms, we shall rewrite it from the efficiencies of the subsystems that constitute the plant.

The solar collector efficiency, η_s, is defined as the ratio between the useful energy per unit time provided by the collector, $|\dot{Q}'_{\mathrm{HS}}|$ (see Fig. 1), and the solar energy rate it receives, GA_a: $\eta_s = |\dot{Q}'_{\mathrm{HS}}|/GA_a$. The solar central tower transfers a fraction of the useful heat collected by the heliostats, $|\dot{Q}'_{\mathrm{HS}}|$, to the working fluid, that is denoted $|\dot{Q}_{\mathrm{HS}}|$. Introducing ε_{HS}, the effectiveness of the solar receiver (considered as a heat exchanger), $|\dot{Q}_{\mathrm{HS}}| = \varepsilon_{\mathrm{HS}}|\dot{Q}'_{\mathrm{HS}}|$, the solar collector efficiency can be expressed as: $\eta_s = |\dot{Q}_{\mathrm{HS}}|/(\varepsilon_{\mathrm{HS}}GA_a)$.

In a similar way the efficiency of the main combustion process, η_{cp}, is defined as the quotient between the heat flux from the combustion chamber and the energy contents of the entering fuel, $\dot{m}_f Q_{\mathrm{LHV}}$. The combustion chamber produces a heat rate, $|\dot{Q}'_{\mathrm{HCp}}|$, transferred to the working fluid through a heat exchanger whose effectiveness is $\varepsilon_{\mathrm{HCp}} = |\dot{Q}_{\mathrm{HCp}}|/|\dot{Q}'_{\mathrm{HCp}}|$, where $|\dot{Q}_{\mathrm{HCp}}|$ is the actual heat rate received by the working fluid from combustion. As a result, the combustion chamber efficiency can be written as:

$$\eta_{\mathrm{cp}} = \frac{|\dot{Q}_{\mathrm{HCp}}|}{\dot{m}_{fp}\,\varepsilon_{\mathrm{HCp}}\,Q_{\mathrm{LHV}}} \tag{4}$$

The combustion efficiency for each intermediate reheater, η_{ci}, is calculated alike:

$$\eta_{\mathrm{ci}} = \frac{|\dot{Q}_{\mathrm{rehi}}|}{\dot{m}_{fi}\,\varepsilon_{\mathrm{rehi}}\,Q_{\mathrm{LHV}}} \tag{5}$$

Each one has an associated heat exchanger with effectiveness, $\varepsilon_{rehi} = |\dot{Q}_{\mathrm{rehi}}|/|\dot{Q}'_{\mathrm{rehi}}|$.

The total heat input rate that the fluid absorbs from combustion is given as:

$$|\dot{Q}_{HC}| = |\dot{Q}_{HCp}| + |\dot{Q}_{reh}| \tag{6}$$

where

$$|\dot{Q}_{reh}| = \sum_{i=1}^{N_t-1} |\dot{Q}_{rehi}| \tag{7}$$

The efficiency of the thermal engine itself, η_h, is the ratio between the mechanical power output and the total heat input rate:

$$\eta_h = \frac{|\dot{W}|}{|\dot{Q}_H|} = \frac{P}{|\dot{Q}_{HS}| + |\dot{Q}_{HCp}| + |\dot{Q}_{reh}|} \tag{8}$$

Thus, the overall system efficiency, η, given by Eq. (1), is:

$$\eta = \frac{P}{\frac{|\dot{Q}_{HS}|}{\varepsilon_{HS}\,\eta_s} + \left[\frac{|\dot{Q}_{HCp}|}{\varepsilon_{HCp}\,\eta_{cp}} + \sum_{i=1}^{N_t-1} \frac{|\dot{Q}_{rehi}|}{\varepsilon_{rehi}\,\eta_{ci}}\right]} \tag{9}$$

Assuming identical efficiencies for the main combustion chamber and for reheaters, $\eta_{cp} = \eta_{ci} \equiv \eta_c$ and $\varepsilon_{HCp} = \varepsilon_{rehi} \equiv \varepsilon_{HC}$, the thermodynamic efficiency can be written as:

$$\eta = \frac{P}{\frac{|\dot{Q}_{HS}|}{\varepsilon_{HS}\,\eta_s} + \frac{|\dot{Q}_{HC}|}{\varepsilon_{HC}\,\eta_c}} = \eta_h\,\eta_s\,\eta_c \left(\frac{|\dot{Q}_{HS}| + |\dot{Q}_{HC}|}{\frac{\eta_c|\dot{Q}_{HS}|}{\varepsilon_{HS}} + \frac{\eta_s|\dot{Q}_{HC}|}{\varepsilon_{HC}}}\right) \tag{10}$$

It is interesting to define a solar share, f, as the ratio between the heat input rate from the sun and the total one:

$$f = \frac{|\dot{Q}_{HS}|}{|\dot{Q}_{HS}| + |\dot{Q}_{HC}|} \tag{11}$$

Depending on solar conditions, the solar share fluctuates in the interval [0,1]. $f = 1$, means that all the heat input has solar origin and $f = 0$ means

that all the heat input comes from combustion, for instance by night. With this definition it is possible to express the overall plant efficiency in terms of the efficiency of the solar subsystem, η_s, that of the combustion chambers η_c, the efficiency of the Brayton heat engine η_h, the *solar share* f, and the effectivenesses of the heat exchangers between subsystems ε_{HS} and ε_{HC}:

$$\eta = \eta_h\,\eta_s\,\eta_c\left[\frac{1}{\frac{\eta_c\,f}{\varepsilon_{HS}}+\frac{\eta_s\,(1-f)}{\varepsilon_{HC}}}\right] = \eta_h\,\eta_s\,\eta_c\left[\frac{\varepsilon_{HS}\,\varepsilon_{HC}}{\eta_c\,f\varepsilon_{HC}+\eta_s(1-f)\varepsilon_{HS}}\right] \tag{12}$$

In the particular case of only solar heat input, $f = 1$, so $\eta = \eta_h\eta_s\varepsilon_{HS}$, and for only combustion $f = 0$, and $\eta = \eta_h\eta_c\varepsilon_{HC}$.

It is interesting to define an efficiency with an economic meaning, the *fuel conversion rate* as the ratio between the power output and the heat input rate with an associated cost [32]:

$$r_e = \frac{P}{\dot{m}_f\,Q_{LHV}} \tag{13}$$

For pure solar operation ($\dot{m}_f = 0$), $f = 1$, and $r_e \to \infty$ and for only combustion operation, $f = 0$, so $r_e = \eta$. It can be expressed in terms of the efficiency of the subsystems and the solar share as:

$$r_e = \frac{\eta\,\eta_s\,\eta_h\,\varepsilon_{HS}}{\eta_s\,\eta_h\,\varepsilon_{HS}-\eta\,f} \tag{14}$$

2.2. Solar subsystem model

Next we briefly summarized the model for the losses and efficiency in the solar subsystem, considered as an heliostat field with aperture area A_a and a central tower receiver with area A_r. The solar power collected in the aperture is $|\dot{Q}_s| = GA_a$. Nevertheless, the energy flux collected at the tower has to include optical losses associated to absorption at the heliostats, shadowing and blocking, spillage, ambient humidity and others. The most simple way to globally account for these effects is by defining an optical efficiency, η_0, so the heat input rate reaching the tower receiver is $|\dot{Q}_r| = \eta_0 GA_a$. Also there are heat transfer losses in the receiver due to convection, conduction and radiation. Heat losses can be expressed as [33, 34]:

$$|\dot{Q}_l| = A_r\alpha\sigma\left(T_{HS}^4 - T_L^4\right) + A_r\overline{U}_L\left(T_{HS}-T_L\right) \tag{15}$$

where α the emissivity of the receiver surface, $\overline{U_L}$ is an overall conduction and convection heat transfer coefficient, and σ the Stefan-Boltzmann constant.

So, $|\dot{Q}'_{HS}| = |\dot{Q}_r - \dot{Q}_l|$, represents the effective heat flux that the receiver could transfer to the working fluid, assuming that it behaves as a heat exchanger. The energy rate finally absorbed by the working fluid considering the effectiveness of the receiver, ε_{HS} is:

$$|\dot{Q}_{HS}| = \varepsilon_{HS} \left\{ \eta_0 G A_a - A_r \left[\alpha\sigma \left(T_{HS}^4 - T_L^4 \right) + \overline{U}_L \left(T_{HS} - T_L \right) \right] \right\} \tag{16}$$

This energy rate, as depicted in Fig. 2 increases the working fluid temperature from T_x to $T_{x'}$ The efficiency of the solar subsystem, η_s, can be written as:

$$\eta_s = \eta_0 [1 - h_1 (T_{HS}^4 - T_L^4) - h_2 (T_{HS} - T_L)] \tag{17}$$

where C is the concentration ratio, $C = A_a/A_r$ and h_1, h_2 are losses parameters, defined as: $h_1 = \alpha\sigma/(\eta_0 GC)$ and $h_2 = \overline{U}_L/(\eta_0 GC)$.

2.3. Combustion subsystem

The maximum energy that could be obtained from combustion is $\dot{m}_f Q_{LHV}$ considering ideal combustion and no losses in the combustion chamber. But actually the useful energy that can be transferred to the working fluid is only a fraction of that energy rate, $\eta_{cp}\dot{m}_f Q_{LHV}$. Moreover, we are considering a closed cycle, so the heat is transferred to the power unit through a heat exchanger associated to the combustion chamber with effectiveness, ε_{HCp}. Thus, the heat rate that is actually released to the working fluid can be written as: $|\dot{Q}_{HCp}| = \varepsilon_{HCp} |\dot{Q}'_{HCp}| = \varepsilon_{HCp}\, \eta_{cp}\, \dot{m}_{fp}\, Q_{LHV}$. The same argument applies for the intermediate reheaters, so:

$$|\dot{Q}_{reh}| = \sum_{i=1}^{N_t - 1} \varepsilon_{rehi} |\dot{Q}'_{rehi}| = \sum_{i=1}^{N_t - 1} \varepsilon_{rehi}\, \eta_{ci}\, \dot{m}_{fi}\, Q_{LHV} \tag{18}$$

Assuming that combustion efficiencies are the same for all the reheaters and equal to that of the main combustion and also that all the associated heat exchangers are similar:

$$|\dot{Q}_{reh}| = \varepsilon_{HC}\, \eta_c\, Q_{LHV} \sum_{i=1}^{N_t - 1} \dot{m}_{fi} \tag{19}$$

2.4. Multi-stage Brayton power unit model

In this section a model for the multi-stage Brayton cycle is proposed and its thermal efficiency, η_h, evaluated. The working fluid is considered

as an ideal gas with temperature dependent specific heats, $c_w(T)$, following an irreversible recuperative Brayton cycle with multiple compression and expansion steps. The temperature-entropy diagram of the cycle is depicted in Fig. 2. In the following the main cycle stages are modeled together with the main irreversibility sources associated to each:

- In the first process ($1 \rightarrow 2$), the working fluid is compressed through an arbitrary number, N_c, of compressors. They are considered identical, so the isentropic efficiency of any of them is: $\varepsilon_c = (T_{2s} - T_1)/(T_2 - T_1)$, where T_{2s} would be temperature after compressions if they were isentropic (see Fig. 2). Between each pair of compressors, it is considered an intercooler, so the inlet temperature of all compressors is the same, T_1.

- Between states 2 and 3, three subsequent heat inputs increase the fluid temperature. First, a non-ideal recuperator increases temperature from T_2 up to T_x. Its effectiveness is defined as: $\varepsilon_r = (T_x - T_2)/(T_4 - T_2) = (T_y - T_4)/(T_2 - T_4)$. A non-recuperative plant is easily simulated by taking $\varepsilon_r = 0$. Second, if solar conditions are good enough, the fluid receives a solar heat input rate, $|\dot{Q}_{HS}|$, that rises up the temperature from T_x to $T_{x'}$. And third, the main combustion chamber provides the required energy to reach the turbines inlet temperature, T_3, that is assumed as a fixed input parameter. So, in principle (apart from fluctuations of the ambient temperature), the only oscillating temperature during heat input due to irradiance oscillations is $T_{x'}$. Although each subprocess during heat input has its own pressure losses, for simplicity we consider a parameter that globally measures the whole pressure losses in the fluid during the heating process, $\rho_H = (p_{\mathrm{H}} - \Delta p_{\mathrm{H}})/p_{\mathrm{H}}$, where p_H is the highest pressure (compressor exit) and $p_{\mathrm{H}} - \Delta p_{\mathrm{H}}$ is the pressure at the first turbine inlet.

- At the state 3 the working fluid attains its maximum temperature and it is expanded by N_t subsequent gas turbines. Any of them is characterized by an isentropic efficiency $\varepsilon_t = (T_4 - T_3)/(T_{4s} - T_3)$. To ensure that the temperature at any turbine inlet is T_3, $N_t - 1$ intermediate reheaters are required. After the last turbine, the fluid reaches state 4.

- Finally, the fluid recovers the conditions of state 1 by means of a heat release that is split in two processes. The first associated to recuperation that ends at temperature T_y and the second through a heat

exchanger that cools the fluid up to T_1. Its effectiveness is defined as: $\varepsilon_{\mathrm{L}} = (T_1 - T_y)/(T_L - T_y)$. The global pressure decay in $4 \to 1$ is measured by introducing a parameter: $\rho_{\mathrm{L}} = (p_{\mathrm{L}} - \Delta p_{\mathrm{L}})/p_{\mathrm{L}}$ where p_L is the fluid pressure after the last turbine and $p_L - \Delta p_L$ the lowest pressure. It is convenient to define an overall pressure ratio as $r_p = p_{\mathrm{H}}/(p_{\mathrm{L}} - \Delta p_{\mathrm{L}})$.

Next, the objective is to obtain cycle temperatures and heat rates in terms of the parameters associated to cycle size and geometry, and thermal losses. By convenience we define two parameters, a_c and a_t, related to pressure ratios of compressors and turbines:

$$a_c = \frac{T_{2s}}{T_1} = \left(\frac{p_{\mathrm{H}}}{p_L - \Delta p_L}\right)^{(\bar{\gamma}_{12}-1)/\bar{\gamma}_{12}} = r_p^{(\bar{\gamma}_{12}-1)/\bar{\gamma}_{12}} \tag{20}$$

$$a_t = \frac{T_3}{T_{4s}} = \left(\frac{p_{\mathrm{H}} - \Delta p_{\mathrm{H}}}{p_L}\right)^{(\bar{\gamma}_{34}-1)/\bar{\gamma}_{34}} \tag{21}$$

In these definitions it was considered that processes $1 \to 2s$ and $3 \to 4s$ are isentropic. $\bar{\gamma}_{12}$ is the mean value of the adiabatic constant in the temperature interval $[T_1, T_2]$ and similarly for $\bar{\gamma}_{34}$. Those temperature intervals are not large, so it is reasonable to work on average values instead of temperature dependent parameters. From the definitions of ρ_H and ρ_L it is easy to show that the overall pressure ratio and a_t are related by:

$$a_t = (\rho_H \rho_L r_p)^{(\bar{\gamma}_{34}-1)/\bar{\gamma}_{34}} \tag{22}$$

From all the assumptions and definitions before it is possible to obtain analytical expressions for all the cycle temperatures after some algebraic calculations:

$$T_1 = \varepsilon_L T_L + T_y\,(1 - \varepsilon_L) \tag{23}$$

$$T_2 = T_1 + \frac{1}{\varepsilon_c}\,(T_{2s} - T_1) = T_1 Z_c \tag{24}$$

$$T_3 = \varepsilon_{\mathrm{HC}} T_{\mathrm{HC}} + T_{x'}\,(1 - \varepsilon_{\mathrm{HC}}) \tag{25}$$

$$T_4 = T_3 - \varepsilon_t\,(T_3 - T_{4s}) = T_3 Z_t \tag{26}$$

$$T_x = \varepsilon_r T_4 + T_2\,(1 - \varepsilon_r) \tag{27}$$

$$T_y = \varepsilon_r T_2 + T_4\,(1 - \varepsilon_r) \tag{28}$$

$$T_{x'} = \varepsilon_{\mathrm{HS}} T_{\mathrm{HS}} + T_x \left(1 - \varepsilon_{\mathrm{HS}}\right) \tag{29}$$

where other two definitions were included:

$$Z_c = 1 + \frac{1}{\varepsilon_c}\left(a_c^{1/N_c} - 1\right) \tag{30}$$

$$Z_t = 1 - \varepsilon_t \left(1 - \frac{1}{a_t^{1/N_t}}\right) \tag{31}$$

By using all these equations, temperatures T_2 and T_4 can be written as functions of the temperatures of the heat sources, T_{HS} and T_{HC}, the ambient temperature, T_L, the overall pressure ratio, r_p and the irreversibility parameters. This leads to:

$$T_2 = \frac{(1-\varepsilon_L)(1-\varepsilon_r)[\varepsilon_{\mathrm{HC}} T_{\mathrm{HC}} + \varepsilon_{\mathrm{HS}} T_{\mathrm{HS}}(1-\varepsilon_{\mathrm{HC}})] + \varepsilon_L T_L \left[Z_t^{-1} - (1-\varepsilon_{\mathrm{HC}})(1-\varepsilon_{\mathrm{HS}})\varepsilon_r\right]}{\left[Z_c^{-1} - (1-\varepsilon_L)\varepsilon_r\right]\left[Z_t^{-1} - (1-\varepsilon_{\mathrm{HC}})(1-\varepsilon_{\mathrm{HS}})\varepsilon_r\right] - (1-\varepsilon_{\mathrm{HC}})(1-\varepsilon_{\mathrm{HS}})(1-\varepsilon_L)(1-\varepsilon_r)^2} \tag{32}$$

$$T_4 = \frac{[\varepsilon_{\mathrm{HC}} T_{\mathrm{HC}} + \varepsilon_{\mathrm{HS}} T_{\mathrm{HS}}(1-\varepsilon_{\mathrm{HC}})]\left[Z_c^{-1} - (1-\varepsilon_L)\varepsilon_r\right] + \varepsilon_L T_L (1-\varepsilon_{\mathrm{HC}})(1-\varepsilon_{\mathrm{HS}})(1-\varepsilon_r)}{\left[Z_c^{-1} - (1-\varepsilon_L)\varepsilon_r\right]\left[Z_t^{-1} - (1-\varepsilon_{\mathrm{HC}})(1-\varepsilon_{\mathrm{HS}})\varepsilon_r\right] - (1-\varepsilon_{\mathrm{HC}})(1-\varepsilon_{\mathrm{HS}})(1-\varepsilon_L)(1-\varepsilon_r)^2} \tag{33}$$

Any other temperature can be obtained in the same terms by substituting Eqs. (32) y (33) in Eqs. (23)-(29).

Now it is feasible to calculate all the components of the heat input rate, $|\dot{Q}_H| = |\dot{Q}_{HS}| + |\dot{Q}_{HCp}| + |\dot{Q}_{reh}|$, by using temperature equations and Eqs. (6) and (7):

$$|\dot{Q}_{\mathrm{HS}}| = \dot{m} \int_{T_x}^{T_{x'}} c_w(T)\, dT = f|\dot{Q}_H| \tag{34}$$

$$|\dot{Q}_{\mathrm{HCp}}| = \dot{m} \int_{T_{x'}}^{T_3} c_w(T)\, dT \tag{35}$$

$$|\dot{Q}_{reh}| = \dot{m} \sum_{j=1}^{N_t - 1} \int_{T_j}^{T_3} c_w(T)\, dT \tag{36}$$

where T_j is the temperature at the exit of turbine j. In order to obtain an analytical expression for the last equation it will be assumed that the difference between T_3 and the temperatures at turbines exit, T_j, is not large,

so a mean value for $c_w(T)$, $\overline{c}_{w,34}$ is considered. This hypothesis allows to write:

$$|\dot{Q}_{reh}| = \dot{m} \sum_{j=1}^{N_t-1} \int_{T_{js}}^{T_3} c_w(T)\, dT \simeq \dot{m}\, \varepsilon_t\, \overline{c}_{w,34} \sum_{j=1}^{N_t-1} (T_3 - T_{js})$$
$$= \dot{m}\, \overline{c}_{w,34}\, \varepsilon_t (N_t - 1)(1 - a_t^{-1/N_t}) T_3 \tag{37}$$

The heat released by the working fluid to the cold source in the closed cycle can be expressed as:

$$|\dot{Q}_L| = \dot{m} \int_{T_1}^{T_y} c_w(T)\, dT + \dot{m} \sum_{k=1}^{N_c-1} \int_{T_1}^{T_k} c_w(T)\, dT \tag{38}$$

Assuming that the difference between T_1 and the temperature at any compressor exit is not large, a mean value of the specific heat, $\overline{c}_{w,12}$, is taken in order to calculate the total heat release rate:

$$|\dot{Q}_L| = \dot{m} \int_{T_1}^{T_y} c_w(T)\, dT + \dot{m} \frac{\overline{c}_{w,12}}{\varepsilon_c} \sum_{s=1}^{N_c-1} (T_{ks} - T_1) \tag{39}$$

The second term at the right side can be calculated as:

$$\dot{m}\, \frac{\overline{c}_{w,12}}{\varepsilon_c} \sum_{s=1}^{N_c-1} (T_{ks} - T_1) = \dot{m} \frac{\overline{c}_{w,12}}{\varepsilon_c} (N_c - 1)(a_c^{1/N_c} - 1) T_1 \tag{40}$$

and finally,

$$|\dot{Q}_L| = \dot{m} \int_{T_1}^{T_y} c_w(T)\, dT + \dot{m} \frac{\overline{c}_{w,12}}{\varepsilon_c} (N_c - 1)(a_c^{1/N_c} - 1) T_1 \tag{41}$$

The power output provided by the plant is then calculated as:

$$P = |\dot{Q}_H| - |\dot{Q}_L| \tag{42}$$

and its thermal efficiency through:

$$\eta_h = \frac{P}{|\dot{Q}_H|} \tag{43}$$

Before finishing this section we recall that from the plant scheme we have assumed (see Fig. 2), the following conditions for the temperatures at the hot side:

$$T_3 \geq T_{x'} \geq T_x \tag{44}$$

$$T_{HS} \geq T_x \tag{45}$$

$$T_{HC} \geq T_{x'} \tag{46}$$

Also, in summary, its worth to note that with respect to the dependence of specific heats with temperature it was assumed that temperature changes in compression ($1 \rightarrow 2$) and expansion ($3 \rightarrow 4$) processes are small so mean values were taken ($\overline{c}_{w,12}$ and $\overline{c}_{w,34}$, respectively). Nevertheless, during heat input and release, of course changes could be large so explicit polynomials for $c_w(T)$ will be taken. These assumptions allow to obtain straightforward analytical expressions for all the temperatures in the cycle and so, to analyze the sensitivity of the performance of the whole plant to any design or irreversibility parameter. Accounted irreversibilities for the thermodynamic engine are external (arising from the coupling of the heat engine to the external heat sources, ε_{HS} and ε_{HC}) and internal (associated to compressors, ε_c, turbines, ε_t, recuperator, ε_t, and pressure losses, ρ_H and ρ_L).

3. Numerical computations

3.1. Design point conditions and model validation

The thermodynamic model presented in this work in the particular case of single stage compression and expansion was applied in previous works by our group in order to predict the performance records of a project developed by *Abengoa Solar* near Seville, Spain, called *Solugas Project* [11, 31]. In this project a natural gas commercial single stage air gas turbine (*Caterpillar Mercury 50*) was modified in order to be hybridized with a central tower solar receiver.

First, the model was validated for the turbine working at full load on an only combustion mode. This turbine operates at a pressure ratio $r_p = 9.9$ with an air gas flow $\dot{m} = 17.9$ kg/s. The turbine inlet temperature is $T_3 = 1423$ K and provides 4.6 MWe fueled with natural gas [30, 35]. The manufacturer reports a thermal efficiency after generator, $\eta_{he} = 0.385$ for $T_L = 288$ K. Our model is capable to reproduce the thermal efficiency of the turbine with a deviation below 0.5% and the power output below

1.5%. The following parameters were assumed in the model: $\varepsilon_{HC} = 0.98$, $\varepsilon_{HS} = 0.78$, $\varepsilon_L = 1$, $\rho_H = \rho_L = 0.97$ (relative global pressure losses about 9.2%), $\varepsilon_c = 0.885$, $\varepsilon_t = 0.815$, and $\varepsilon_r = 0.775$. Details on the calculations and explicit tables with the parameters can be found in [30].

The plant developed for the Solugas project was also simulated operating in hybrid conditions at design point solar irradiance ($G = 860$ W/m^2) and ambient temperature ($T_L = 288$ K). The parameters considered for the solar subsystem are: $\eta_0 = 0.73$, $\alpha = 0.1$, $\varepsilon_{HS} = 0.95$, $C = 425.2$, and $\overline{U}_L = 5$ W/(m^2 K). In these conditions the model (considering dry air with temperature dependent specific heat) predicts an overall plant efficiency, $\eta = 0.32$, a fuel conversion efficiency, $r_e = 0.58$, a solar share $f = 0.32$, a specific fuel consumption, $m_f = 132$ kg/(MW h), and a mechanical power output $P = 5.06$ MW. The objective of this work is focused on the analysis of the model predictions if the single stage gas turbine was substituted by a multi-step one, and also on the influence of other possible working fluids, different from air. In the next subsection we motivate the interest of using different working fluids in the search for improved plant performance. The basic parameters of the Solugas plant will be assumed as reference values.

3.2. Working fluids

The advantages of closed gas turbines when comparing with open ones and Rankine cycles are diverse [7, 36]: closed-cycle gas turbines at high temperatures can reach efficiencies similar to steam cycles, lead to simpler plant designs (less number of heat exchangers, pumps, and piping), and have more compact components and so lower size for a fixed rated power output. Moreover, unlike open-cycle Brayton plants can use dirty fuels as biomass and other heat sources (nuclear and solar for instance). And moreover, different working fluids (depending on their thermal and transport properties, and practical issues) can be used. This work is focused on the last point.

Among the working fluids that have been used in closed-cycle prototype or real installations, the most usual are: air, nitrogen, helium, carbon dioxide, other noble gases as argon and neon, and also gas mixtures [7]. Main advantages of air closed-cycle plants are the wide design experience and practice and, of course, that air is inexpensive and abundant. On the contrary, these plants have considerable pressure losses, require high turbine inlet temperatures that contribute to materials oxidization, and air has a low heat

	He	N_2	Dry air	CO_2
M (g/mol)	4.00	28.01	28.97	44.01
T_c (K)	5.1953	126.19	132.84	304.13
p_c (bar)	2.2761	33.958	38.501	73.773
a	20.7862	32.3518	38.6449	25.4812
b	–	-0.02031	-0.044282	0.051549
c	–	4.2182×10^{-5}	7.9699×10^{-5}	-2.7778×10^{-5}
d	–	-2.7814×10^{-8}	-5.3556×10^{-8}	4.6551×10^{-9}
e	–	6.3098×10^{-12}	1.2726×10^{-11}	4.81185×10^{-13}
$\bar{\gamma}$	1.6667	1.3561	1.3458	1.1986
$\bar{c}_w$ [J/(g K)]	5.1965	1.1354	1.1202	1.1587

Table 1: Thermodynamic properties of the considered working fluids: molecular weight (M), critical temperature and pressure (T_c and p_c respectively) and mean values of the constant pressure specific heat ($\bar{c}_w$) and adiabatic coefficient ($\bar{\gamma}$), in the temperature interval $[288, 1430]$ K. The coefficients of the fits of $c_w(T)$ (in units of J/(mol K)) correspond to the function: $c_w(T) = a + b\,T + c\,T^2 + d\,T^3 + e\,T^4$. Data for the fits were taken from [37] at a pressure $p = 5$ bar.

transfer coefficient. For nitrogen considerations are similar because the experience from air turbines can be applied and most properties are alike. One difference with air is the behavior of materials at high temperatures that in this case nitrides instead of oxidizes.

The use of helium is related with the development of nuclear reactors. References [7, 38] give a detailed historical review of several facilities of this type. Helium is inert and non-toxic, has a good heat transfer coefficient, and low pressure losses. As drawbacks we highlight that turbomachinery design experience is not so broad as for air, requires high turbine inlet temperature, leakage is high, and actually more number of turbomachinery stages are required [39].

Carbon dioxide has been used as working fluid for closed Brayton cycle plants from 1950, mainly partially condensed or supercritical. From late 1990s and early 2000s there have been a renewed interest because research and development work has rapidly evolved turbomachinery and heat exchangers. A recent review has been published by Crespi *et al.* [40]. Solar applications are being also investigated and analyzed nowadays [12, 25, 41, 42]. CO_2 is non-toxic and inert, has a favorable critical point and in supercritical conditions turbomachinery is small and compact and gives good efficiencies

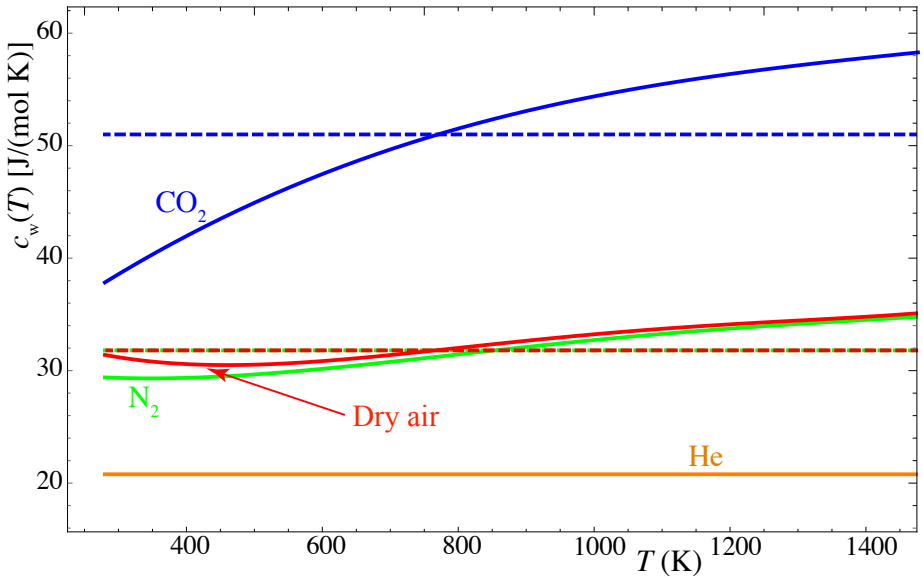

Figure 3: Evolution with temperature of the constant pressure molar heats of the working fluids considered in the work. Average values are shown in dashed lines. Data were taken from [37] at a pressure $p = 5$ bar.

at moderate turbine temperatures. Similarly to helium, design experience is not wide. Moreover, thermodynamic properties vary considerably in the vicinity of the critical point, so detailed investigation on compressors, turbines and other machinery is required. Nevertheless, works on subcritical CO_2 with solar applications are scarce. We highlight the work by Najjar *et al.* [36].

In our study four working fluids are considered: air, nitrogen, helium, and carbon dioxide. Table 1 contains several thermodynamic properties relevant to the application of our model as critical point conditions and evolution with temperature of molar heat, that is plotted in Fig. 3. The figure shows that carbon dioxide has a molar heat about twice larger that a monoatomic gas like He and that its dependence with temperature in the interval from ambient temperature to the temperature at turbine inlet is large. Air and N_2 are in between CO_2 and He. The dependence of their $c_w(T)$ with temperature is not large in the operation interval.

Figure 4 displays a $p-T$ diagram with the liquid-vapor coexistence curve and the approximate processes experienced by the fluids in the Brayton cycle (in the single stage case). It was assumed atmospheric pressure at compres-

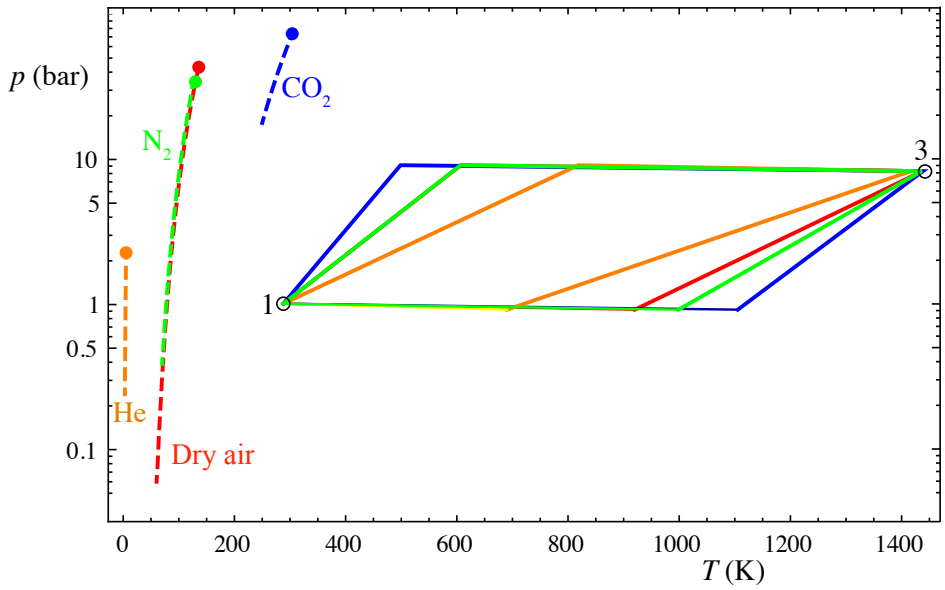

Figure 4: $p - T$ approximate diagrams of the Brayton cycles followed by the considered working fluids. The vertical axis is represented in logarithmic scale. Dashed lines represent the liquid-vapor coexistence lines. Critical points for each fluid are shown as filled circles.

sor inlet and a pressure ratio of 9.9 as in the Solugas project. Within these hypotheses, the considered gases are in subcritical conditions except for He, that performs a transcritical cycle because pressure of states 2 and 3 are above the critical pressure. The aim of our work is to analyze the influence of the working fluid on the performance of the plant from a purely thermodynamic model. It is noteworthy to mention that technical issues related to piping and turbomachinery design are not considered in detail. We assume pressure drops in the cycle and isentropic efficiencies for compressors and turbines similar for all fluids. And also the same pressure at the compressor inlet and the same global plant size (working fluid mass flow). Although from a technical engineering viewpoint an exhaustive study of the mentioned issues would be imperative, we intend to investigate the role played by the thermodynamic properties of the fluids, specially that played in the heat absorption and heat release processes through the molar heat, $c_w(T)$. In consequence conclusions about the influence of the working fluid on plant output records, for different plant layouts in terms of the number of compression/expansion processes at similar conditions, can be extracted.

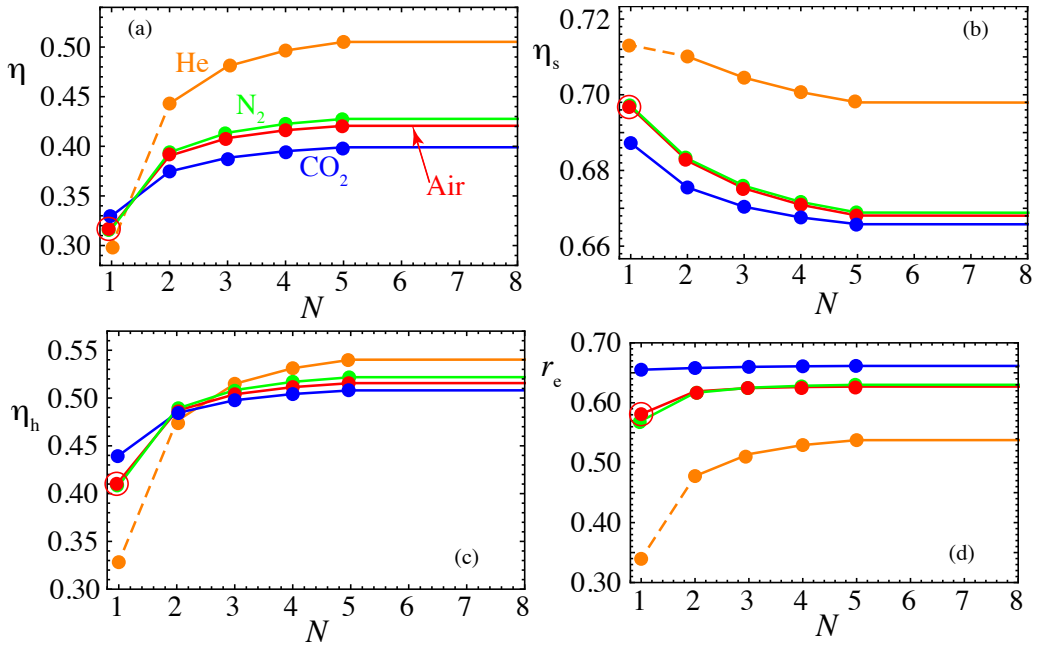

Figure 5: Evolution of plant efficiencies (η, overall plant efficiency; η_s, solar subsystem efficiency; η_h, heat engine efficiency; and r_e, fuel conversion rate) with the number of compression/expansion stages assumed identical, $N_t = N_c \equiv N$, for all the fluids considered. The reference values corresponding to the Solugas project are marked with an open circle. Lines between points are just a guide for the eye. Lines are dashed for He between N=1 and the other cases because for N=1 no regeneration is considered. The input data are those in Sec. 3.

4. Numerical predictions on plant performance

Model predictions within the considerations detailed in the previous section are presented hereafter. Most significant plant efficiencies are plotted in Fig. 5 in terms of the number of compression, N_c, and expansion steps, N_t, assumed identical: $N_t = N_c = N$. In all the plots the reference values corresponding to the Solugas project (air as working fluid and $N = 1$) are marked with an open circle. Table 2 displays the relative increments with respect to that case. For instance, in the case of air, when considering two compressors with intercooling and two turbines with reheating ($N = 2$), the overall plant efficiency, η, experiences an increase about 23% with respect to $N = 1$. The addition of more compression/expansion stages could increase overall efficiency up to 37% approximately.

The evolution of the global efficiency curves for all fluids are similar: a

rapid increase from $N = 1$ to $N = 2$ or 3 and a subsequent slower increase up to an asymptotic value. This evolution for the overall efficiency, η (Fig. 5(a)), comes essentially from that of the Brayton heat engine, η_h, displayed in Fig. 5(b). The behavior of air and nitrogen is similar, although the curve for nitrogen is slightly above that for air. On the contrary, CO_2 shows values for η larger than those for air or nitrogen for $N = 1$, but the increase with the number of compression/expansion stages is slower. The case of He is different. First, for the case N=1 no regeneration was considered. This is due that for the considered pressure ratio (assumed for all the fluids at the design point of Solugas project) is too high for regeneration to be advantageous (see the graph corresponding to He in Fig. 4). We will be back to this point below, when presenting the plots for cycle temperatures. And second, the overall efficiencies for $N \geq 2$ are quite above those for air or nitrogen. For instance, for $N = 2$, η increases about 39% with respect to the reference case for He and 23% for air or nitrogen. This larger values of η for He are essentially associated to the values of the solar subsystem efficiency, η_s (Fig. 5(c)), that are larger for He (we shall return this point when presenting the results for temperatures). The values of η_h for helium are above those for air but only slightly for $N \geq 3$.

The evolution of solar subsystem efficiencies, η_s, with N displays a monotonic decreasing behavior because the operating temperatures of the solar collector increases with N and so losses become larger. Anyway, the interval of numerical values in which η_s evolves is quite narrow (see the vertical axis in the plot for η_s). The behavior of the fuel conversion rate, r_e (the ratio between the power output and the heat input with an economic cost), is quite diverse and interesting (Fig. 5(d)). r_e is larger for CO_2 that for the other fluids, and it is almost independent of N. These values are about 13% over that for the reference case (see Table 2). Nevertheless, for air, N_2 and He, r_e increases with N. The poorest values of r_e are those for helium.

Working fluid	Dry Air		N_2			He			CO_2		
N	2	$N \to \infty$	1	2	$N \to \infty$	$1^{(\mathrm{NR})}$	2	$N \to \infty$	1	2	$N \to \infty$
η	22.623	36.956	-0.560	23.713	39.868	-5.894	39.132	67.745	3.577	17.656	29.970
η_h	17.967	28.476	-0.985	18.489	30.611	-20.427	15.373	38.138	6.655	17.388	26.674
η_s	-2.026	-6.030	0.0593	-1.941	-5.894	2.359	1.932	-1.986	-1.352	-3.037	-5.563
r_e	6.531	8.119	-1.921	6.139	9.180	-41.557	-17.778	-2.833	12.768	13.262	14.245

Table 2: Percentage relative variations of the estimated efficiencies with respect to the reference values of the Solugas project (points marked with an open circle in Fig. 5). In the case of He and N=1, no regeneration is considered (NR). The pressure ratio was taken in all cases as in the gas turbine of the Solugas project, $r_p = 9.9$. The case of a large number of compression/expansion stages is represented as $N \to \infty$.

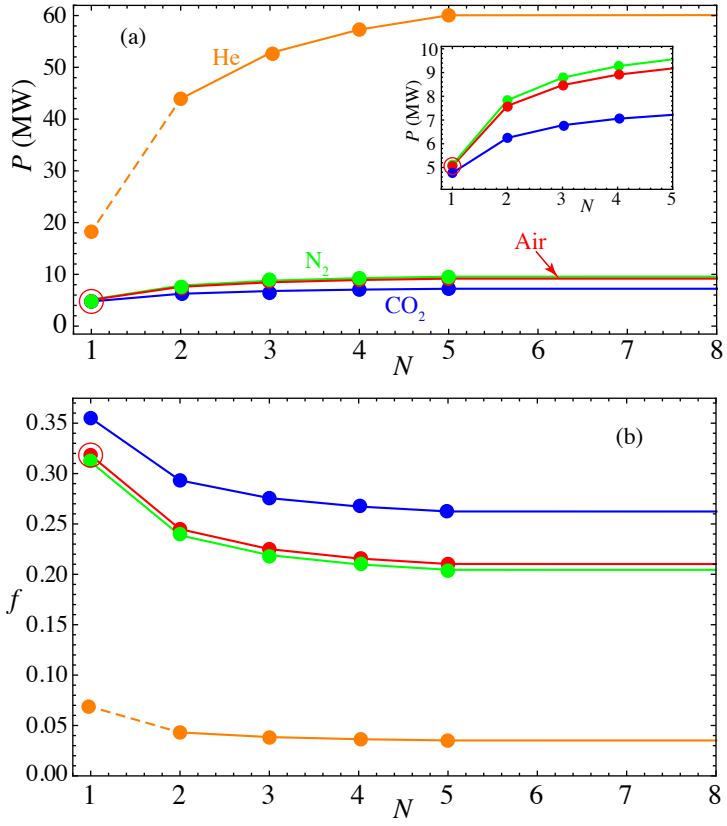

Figure 6: Evolution of the power output, P, and the solar share, f, with N. Open circles show the values corresponding to the reference Solugas plant. The inset shows a zoom with the behavior of air, N_2, and CO_2 with changing values of N.

The power output is much larger for He that for the other fluids as displayed in Fig. 6(a). This is an effect associated to the conditions in which we are comparing the results for the different fluids. Helium has a molar mass much lower than air or the other fluids and on the contrary a constant pressure specific heat about 4 times larger than them (see the mean values in Table 1). The numerical magnitude of power output is proportional to $\dot{m}c_w$. As we are assuming that the working fluid mass flow is the same for all fluids, power output for He is for $N = 1$ larger than for the rest of considered fluids in the same proportion that c_w. This effect is amplified for larger values of N due to the heat input in the reheaters between turbines. For the other fluids power output increases with N up to approximately $N = 3$. For larger N power output remains almost constant. The increase is larger

for air and nitrogen. The inset in the figure shows that for $N \geq 2$ expected power output is larger for N_2 than for air.

The solar share, f, (Fig. 6(b)) decreases for all fluids with the number of compression/expansion stages. This is associated to the increase of heat input from combustion in the intermediate reheaters between turbines. Largest solar share is observed for CO_2 and $N = 1$, where $f \simeq 0.35$. On the other side, solar heat input for helium is always very small.Thus, in order to increase the fluid temperature from the compressor outlet to the turbine, the heat input from the combustion chamber is the most important term. The solar subsystem size (aperture area) in the reference plant is undersized for He and in consequence, the fuel conversion efficiency, r_e, is low.

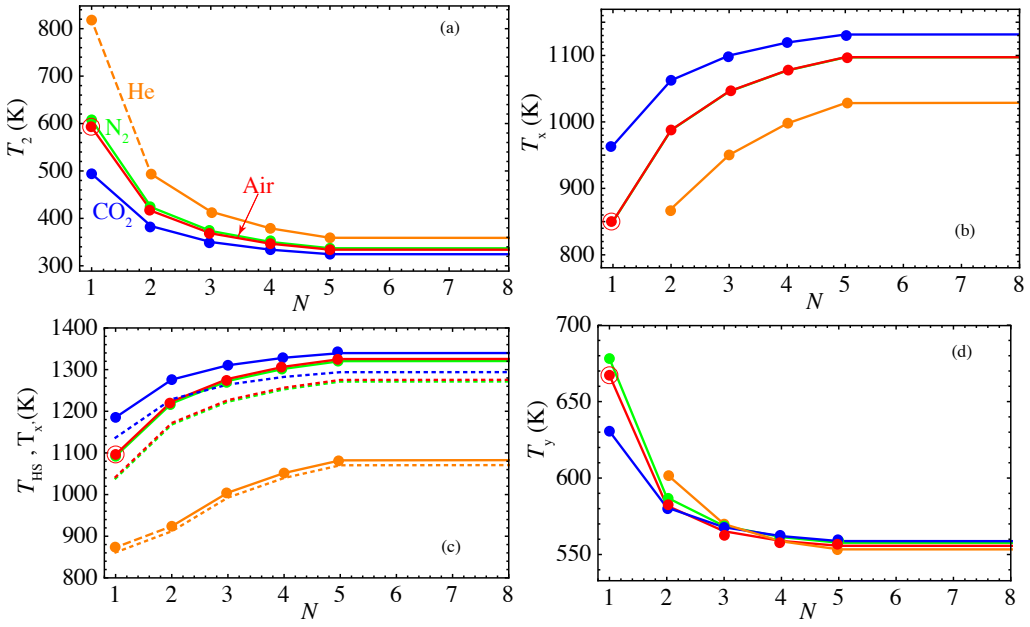

Figure 7: Sensitivity of some plant temperatures to N: T_2, compressors outlet temperature; T_{HS}, solar collector working temperature; $T_{x'}$, temperature of the fluid after absorbing the solar heat (shown in dotted lines in the bottom left plot); T_x, fluid temperature after regeneration; and T_y, gas temperature at the output of the regeneration hot stream. Open circles show the values corresponding to the reference Solugas plant. In the case of He and N=1 no regeneration is considered so the corresponding points in T_x and T_y does not appear in the plots.

Several cycle temperatures are depicted in Fig. 7. The temperature at the compressors exit, T_2 decreases with N and reaches very high values for

He, especially for $N = 1$. This is the reason why regeneration in this case (for the considered value of the pressure ratio, $r_p = 9.9$) is meaningless. For all the fluids, as N increases, the values of T_2 decrease, because intercooling between compressors makes the temperature decrease before the fluid enters the following compressor. The effective temperature of the solar collector, $T_{\rm HS}$ and the temperature the fluid reaches after the solar heat input, $T_{x'}$ always increase con N and are larger for CO_2. Except for He, all numerical values are above 1000 K. Lowest values are reached for He. From the viewpoint of the solar receiver, this means that helium is a good refrigerant. Temperatures of the fluids after regeneration in the cold part of the cycle, T_y, are relatively high in all cases, although decrease with N. This makes feasible to combine the Brayton cycle with a bottoming one as a Rankine in order to take advantage of residual heat. This conclusion is valid for any working fluid.

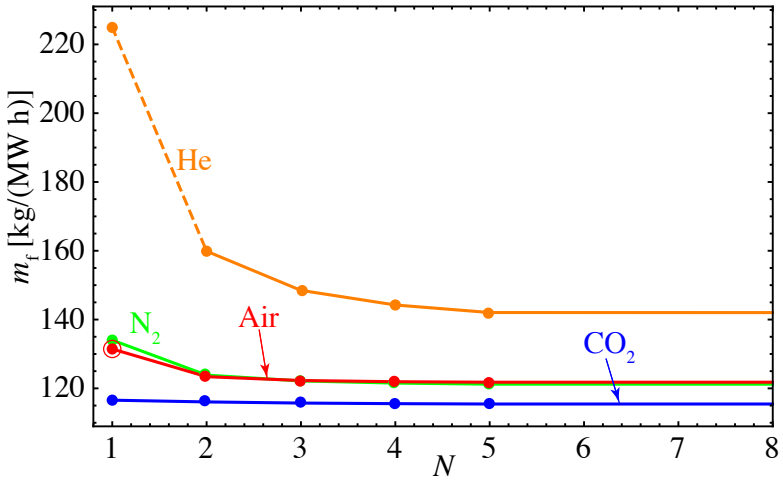

Figure 8: Specific fuel consumption as a function of N. The open circle shows the value corresponding to the reference Solugas plant.

Specific fuel consumption, m_f, assuming natural gas fueling is shown in Fig. 8. Fuel consumption is larger for He, specially for $N = 1$, where no regeneration is assumed. For N_2 and air, the model predicts about 135 kg/(MW h) for $N = 1$ and smaller values for larger N. The main reduction is got in the change from $N = 1$ to $N = 2$. In the case of CO_2, m_f is almost constant. Its numerical value is around 115 kg/(MW h). The fact that in all cases m_f decreases with N means that in spite of the fueling required

by intermediate reheaters, the cycles takes advantage of regeneration. This is shown by the increasing behavior of the temperature of the fluids after regeneration in the heat absorption process, T_x (plot at the top right in Fig. 7).

5. Optimum pressure ratios for each fluid

Up to now we have assumed the same pressure ratio for all fluids, particularly we took the experimental one, $r_p = 9.9$, of the gas turbine employed in project Solugas. The aim of this section is to analyze simultaneously three ingredients in order to seek for optimum plant designs: working fluids, number of compression/expansion steps, and overall pressure ratio. Different efficiencies have been calculated considering the pressure ratio as a variable up to $r_p = 20$.

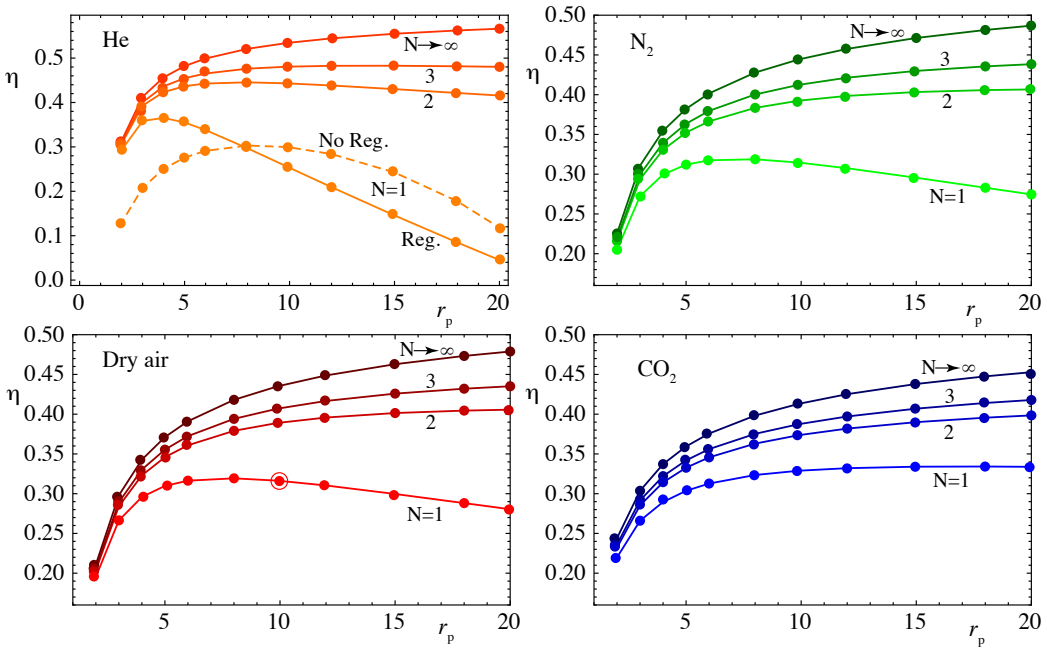

Figure 9: Overall plant efficiency plotted against the pressure ratio for the considered working fluids. Several multi-step configurations are considered. In the case of He and $N = 1$ (top left figure) regenerative (solid line) and non-regenerative plant configurations are plotted (dashed line). The reference efficiency of the Solugas plant is shown for air as an open circle.

Overall plant efficiency is displayed in Fig. 9. In the case of He two configurations were checked for $N = 1$, with and without regeneration. When regeneration is considered, optimum pressure ratios leading to the highest efficiencies are around $r_p = 4$, leading to $\eta \simeq 0.37$. Values of r_p above 8 leads to worse efficiencies than for the non-regenerative configurations. The highest value of η in the case $N = 1$ when regeneration is not incorporated is obtained for $r_p = 8$, $\eta = 0.31$. This means that the incorporation of regeneration increases overall efficiency about 20%, provided that a lower value of the pressure ratio is considered.

For air and nitrogen the curves for η monotonically increase with r_p except for the single stage configuration, where there is a quite flat maximum between values of r_p in the interval $6 - 10$. In the case of CO_2 always an increase of the pressure ratio leads to larger values of efficiency, although for $N = 1$, η is almost constant above $r_p \simeq 10$.

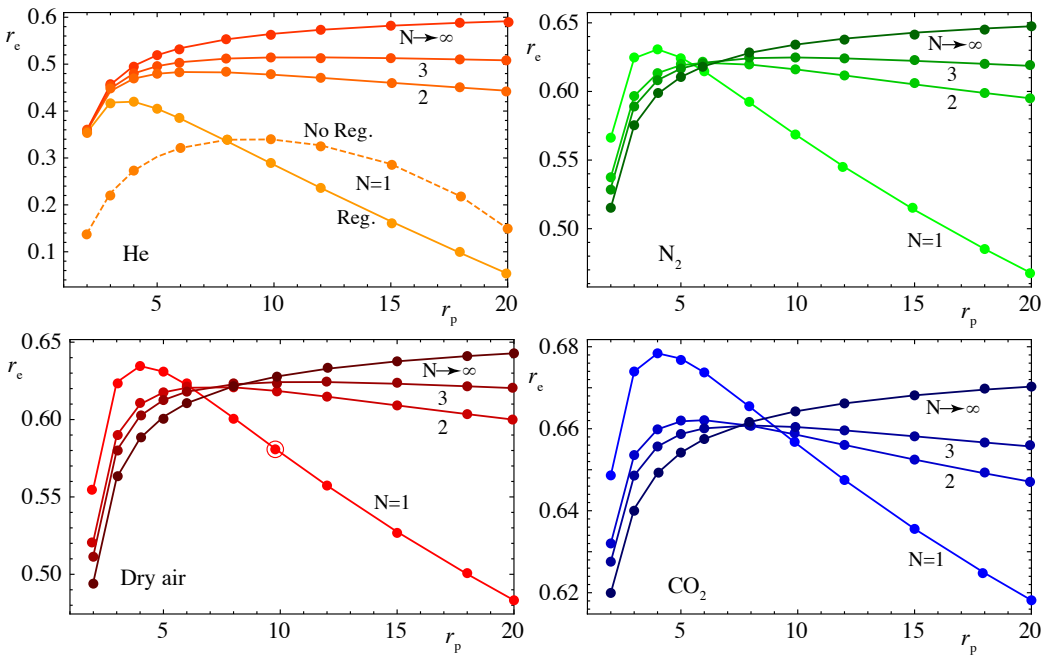

Figure 10: Fuel conversion rate, r_e, against the pressure ratio, r_p for the considered working fluids. In the case of He and $N = 1$ (top left figure) regenerative (solid line) and non-regenerative plant configurations are plotted (dashed line).

Fuel conversion rate, r_e, for all the working fluids, has a narrow maximum (see Fig. 10) for low values of r_p. For He this maximum is below the values

of r_e for multi-stage configurations. Curves of η and r_e are very similar due to the scarce solar heat input for this fluid with the considered aperture area. On the other side, for CO_2, r_e for $N = 1$ is larger than for any other configuration and any other value of the pressure ratio ($r_e = 0.68$). Air and nitrogen are intermediate cases: values of r_e for $N = 1$ and low r_p are similar than those for multi-stage configurations and larger r_p values. For configurations with $N \geq 2$ there is a wide interval of values of r_p leading to good fuel conversion rates. Except for He, small r_p values lead to higher values of r_e for plant layouts with N small. As r_p increases an inversion point is reached (r_p between 6 and 8, depending on the fluid) from which higher N leads to higher values of r_p, *i.e.*, the increase on power output compensates the increase of fuel consumption.

Figure 11 contains the evolution of the power output curves. These curves are always monotonic for multi-stage configurations. For $N = 1$, air and nitrogen display a shallow maximum about $r_p \simeq 10$. This point corresponds to the design point of Solugas project. Helium shows a maximum for $r_p \simeq 5$.

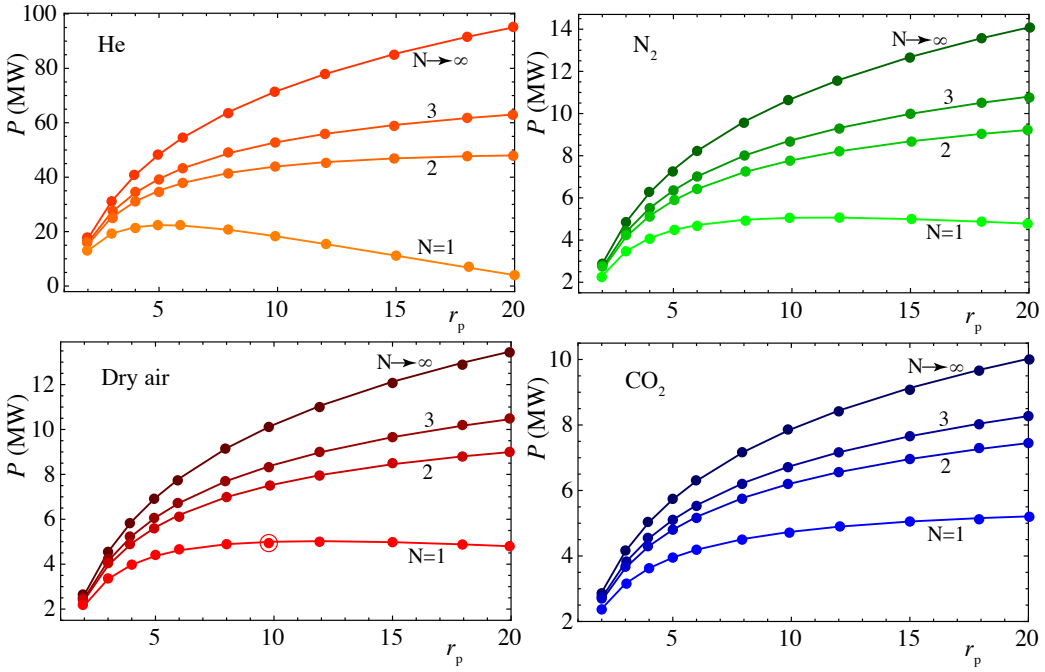

Figure 11: Power output, P, against the pressure ratio, r_p for the considered working fluids.

Figures for the specific fuel consumption, m_f, are not shown because are essentially the reversal of those for r_e. The maxima turn to be minima and the increasing behavior of most curves with r_p turns to be decreasing. To have a numerical idea, minimum m_f is got for CO_2, $N = 1$ and $r_p = 5$, $m_f = 108$ kg/(MW h). For air and nitrogen minimum fuel consumption is reached at similar conditions and is about 120 kg/(MW h).

6. Predictions for two-stages compression cycles

In the previous section was shown that there exist a considerable increase on plant output records from single-stage configurations to two-stage configurations. The subsequent improvement for a higher number of compression/expansion steps is not so noticeable. Thus, in this section particular predictions for two different plant layouts with two compressors and intercooling ($N_c = 2$) are presented: two-stages expansion with reheating ($N_t = 2$) and single-stage expansion ($N_t = 1$). As a function of the pressure ratio, the overall plant efficiency, η, for each fluid is always smaller for single expansion (see Fig. 12(a)) than for two-stages expansion, irrespectively of the working fluid. But it is noteworthy that for air and nitrogen the curves in the case of $N_t = 1$ have a maximum around $r_p = 12$, whereas for $N_t = 2$ are monotonic in all the surveyed interval for r_p. In the case $N_t = 2$, overall efficiency can reach values slightly above 0.4 for air and nitrogen at $r_p \simeq 20$. For $N_t = 1$, $\eta_{\max}$ can be about 0.36 - 0.38, depending on the fluid (see Table 3 for precise values). The power block efficiency, η_h, can attain values around 0.5 for $N_t = 2$ and $r_p \simeq 20$, and 0.46 for air or nitrogen for $N_t = 1$ at $r_p \simeq 10$.

Fuel conversion efficiency, r_e (see Fig. 12(d)) behaves differently that overall efficiency. It is always larger (except for He) for $N_c = 2$, $N_t = 1$ than for $N_c = N_t = 2$. Carbon dioxide leads to the best values of fuel conversion efficiencies, specially for $N_c = 2$, $N_t = 1$ at low values of r_p and also gives reasonable good values of overall efficiency and low specific fuel consumption (see also Fig. 13): $r_{e,\max} = 0.70$ and $m_{f,\min} = 108$ kg/(MW h). Comparing with air and nitrogen (that give similar numbers) in the same conditions, carbon dioxide improves fuel conversion efficiency by 7.7% and decreases specific fuel consumption by 8.5%. And comparing with the reference plant, Solugas, overall efficiency increases 18.7%, fuel conversion efficiency 22.8%, and specific fuel consumption diminishes 22.2%.

With respect to helium, in spite of the probably small size of the heliostat field taken from the reference plant, overall efficiency could take values about

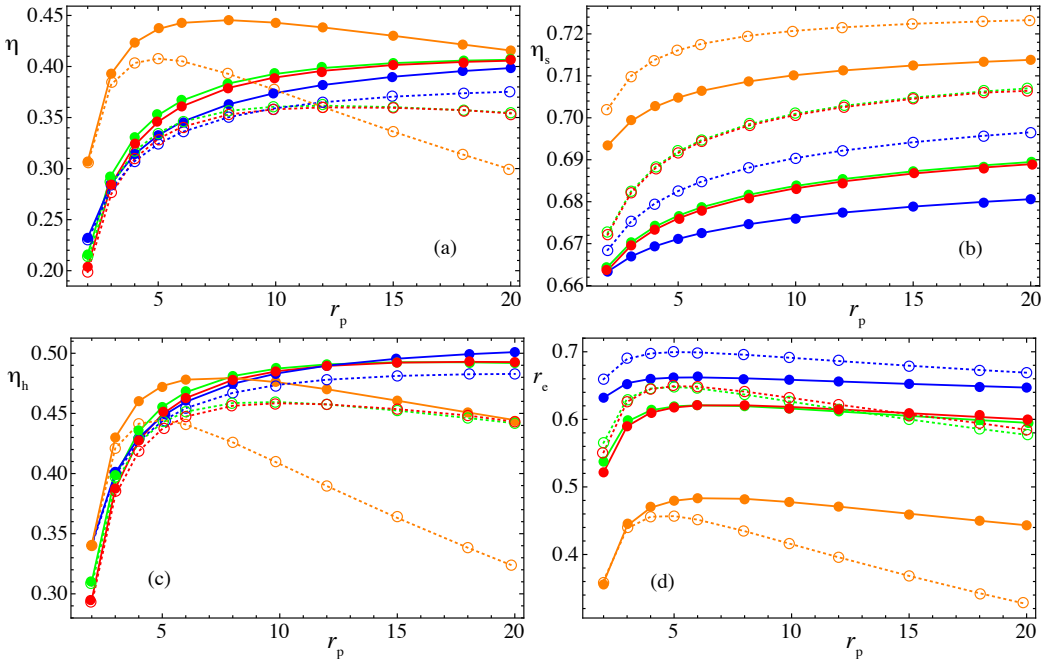

Figure 12: Plant efficiencies as functions of the pressure ratio for different working fluids (helium, orange; dry air, red; nitrogen, green, and carbon dioxide, blue) and two particular configurations: $N_t = N_c = 2$ (solid lines) and $N_t = 1$; $N_c = 2$ (dashed).

0.45 for $N_t = N_c = 2$ and $r_p = 8$, and about 0.40 for $N_t = 1$, $N_c = 2$ and $r_p = 5$. Fuel conversion rate is expected to be around 0.40 - 0.45, that are numbers considerable smaller than those for air or carbon dioxide.

7. Conclusions

In this work a general thermodynamic model for central tower hybrid Brayton thermosolar plants has been developed. The model is capable to predict overall plant performance and other records in terms of the efficiencies of its subsystems: solar field and receiver, Brayton heat engine, and combustion chamber. All the main irreversibility sources are included in the model and it allows to analyze multi-stage compression and expansion and recuperative or non-recuperative layouts. The model considers temperature dependent specific heats of the working fluid. The main heat transfers and so, efficiencies and power output, can be obtained in an analytical way. The most important loss or irreversibility sources are incorporated to the model.

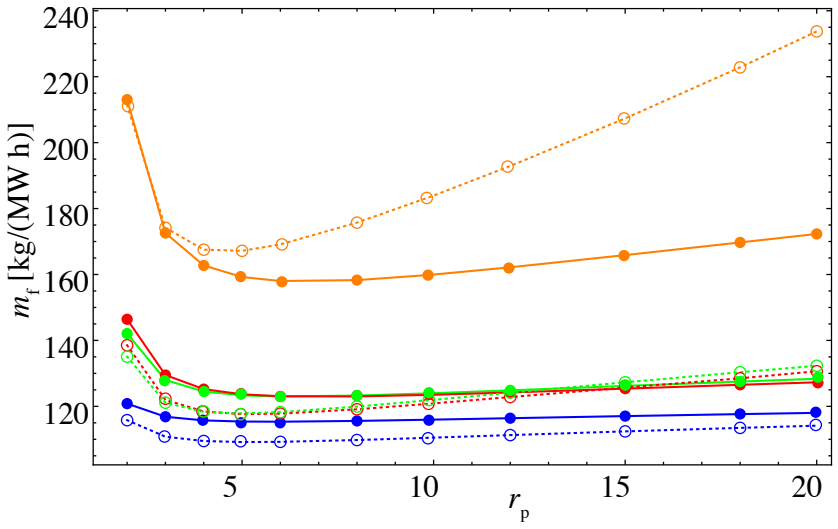

Figure 13: Specific fuel consumption in terms of the pressure ratio for different working fluids (helium, orange; dry air, red; nitrogen, green, and carbon dioxide, blue) and two particular configurations: $N_t = N_c = 2$ (solid lines) and $N_t = 1$; $N_c = 2$ (dashed).

For the Brayton subsystem both internal and external irreversibility sources are considered. Output parameters depend on a not large number of parameters with clear physical meaning, so it is feasible to develop sensitivity analysis and propose optimum plant configurations.

The model is validated by considering a real prototype plant of about 5 MW at design conditions (*Solugas* project, Seville, Spain) as target. Numerical results are presented for several working fluids. First, a fixed overall pressure ratio is considered ($r_p = 9.9$) and the influence of four gas working fluids at subcritical conditions (dry air, nitrogen, carbon dioxide, and helium) analyzed for different multi-stage configurations. Two stage compression and expansion configurations using air, nitrogen or CO_2 as working fluids are capable to increase overall plant efficiency about 17 - 20 % with respect to the reference plant (Solugas). In the case of helium, overall efficiency increases up to 40% but with a large increase of fuel consumption due to reheaters between turbines. In this case, the aperture area of the solar field taken as reference is undersized and solar share small. For the other fluids, the increase of power output associated to multi-stage compression and expansion compensates the increase of fuel consumption and so, the fuel conversion rate improves. Also numerical values with larger number of compression and

	$\eta_{\max}$	r_p	$r_{e,\max}$	r_p	$P_{\max}$ (MW)	r_p	$m_{f,\min}$ [kg/(MW h)]	r_p
Ref.	0.32	9.9	0.58	9.9	5.06	9.9	132	9.9
$N_c = N_t = 2$								
Dry air	0.41	20	0.62	6	9.0	20	121	6
N_2	0.41	20	0.62	6	9.2	20	121	6
He	0.45	8	0.48	6	48.0	20	158	6
CO_2	0.40	20	0.66	6	7.4	20	118	6
$N_c = 2,\ N_t = 1$								
Dry air	0.36	12	0.65	5	6.4	20	118	5
N_2	0.37	12	0.65	5	6.6	20	118	5
He	0.41	5	0.45	5	29.3	8	170	5
CO_2	0.38	20	0.70	5	6.1	20	108	5

Table 3: Maximum values of overall efficiency ($\eta_{\max}$), fuel conversion efficiency ($r_{e,\max}$), maximum power output ($P_{\max}$) and minimum specific fuel consumption ($m_{f,\min}$) and the corresponding pressure ratios for cycles with $N_c = 2$ and one ($N_t = 1$) or two ($N_t = 2$) expansion stages. The reference values of the Solugas project, denoted as (Ref.), are included for comparison.

expansion steps are presented well as the theoretical limits in the eventual case of an arbitrary large number of stages.

Afterwards an analysis of optimum plant configurations is performed. Three ingredients are analyzed together: the working fluid, the number of compression/expansion steps, and the overall pressure ratio. For single stage layouts, the curves of the overall plant efficiency, η, when plotted against the pressure ratio, r_p, have a maximum between $r_p = 5 - 8$ except for CO_2, but for multi-stage configurations, η increases monotonically with r_p for all fluids. The fuel conversion rate, that represents the plant power output with respect to the energy input with an economic cost (fuel consumption), has a maximum for single stage configurations, $N_t = N_c = 1$, at low values of pressure ratio, $r_p \simeq 4 - 5$. These maxima values are high, especially for CO_2 that reaches almost 0.68. For this fluid, subcritical CO_2, the region $r_p \simeq 3 - 7$ is very favorable to get good fuel conversion rates.

An specific analysis was done for two-stages compression cycles ($N_c = 2$) including single-stage expansion ($N_t = 1$) and two-stages expansion ($N_t = 2$). The overall efficiency is larger with $N_t = 2$, but this is opposite for the fuel

conversion rate, r_e. The fluid leading to higher values of r_e is again CO_2 with $N_c = 2$ and $N_t = 1$, that attains $r_e \simeq 0.7$ at $r_p \simeq 5$. Comparing with the data of the reference plant (*Solugas*, single stage, and working with air at $r_p = 9.9$), overall efficiency increases 18.7%, fuel conversion rate increases about 22.8%, and specific fuel consumption decreases about 8.5%, giving values about 108 kg/(MW h). These numbers suggest that the use of subcritical CO_2 with two compressors, intercooling, and single stage expansion could be an interesting option for future plant designs. Although, of course a technical study about turbomachinery details and also about other engineering and economical issues should be developed.

Acknowledgements

Financial support from University of Salamanca and Junta de Castilla y León (project SA017P17) is acknowledged.

[1] M. Dunham, B. Iverson, High-efficiency thermodynamic power cycles for concentrated solar power systems, Renew. Sust. Energ. Rev. 30 (2014) 758–770.

[2] E. Okoroigwe, A. Madhlopa, An integrated combined cycle system driven by a solar tower: a review, Renew. Sust. Energ. Rev. 57 (2016) 337–350.

[3] S. Pramanik, R. V. Ravikrishna, A review of concentrated solar power hybrid technologies, Appl. Therm. Eng. 127 (2017) 602–637.

[4] J. H. Peterseim, S. White, A. Tadros, U. Hellwig, Concentrated solar power hybrid plants, which technologies are best suited for hybridisation?, Renew. Ener. 57 (2013) 520–532.

[5] G. J. Nathan, M. Jafarian, B. B. Dally, W. L. Saw, P. J. Ashman, E. Hu, A. Steinfeld, Solar thermal hybrids for combustion power plant: A growing opportunity, Prog. Ener. Comb. Sci. 000 (2017) 1–25.

[6] K. M. Powell, K. Rashid, K. Ellingwood, J. Tuttle, I. B. D., Hybrid concentrated solar thermal power systems: A review, Renew. Sust. Ener. Rev. 80 (2017) 215–237.

[7] O. Olumayegun, M. Wang, G. Kelsall, Closed-cycle gas turbine for power generation: a state-of-the-art review, Fuel 180 (2016) 694–717.

[8] C. K. Ho, B. D. Iverson, Review of high-temperature central receiver designs for concentrating solar power, Renew. Sust. Energ. Rev. 29 (2014) 835–846.

[9] A. del Río, R. Korzynietz, J. A. Brioso, M. Gallas, I. Ordoñez, M. Quero, C. Díaz, Soltrec - Pressurized volumetric solar air receiver technology, Energ. Proc. 69 (2015) 360–368.

[10] N. Jelley, T. Smith, Concentrated solar power: recent developments and future challenges, J. Power and Energy 229 (2015) 693–713.

[11] R. Korzynietz, J. A. Brioso, A. del Río, M. Quero, M. Gallas, R. Uhlig, M. Ebert, R. Buck, D. Teraji, Solugas - comprehensive analysis of the solar hybrid Brayton plant, Sol. Ener. 135 (2016) 578–589.

[12] J. D. Osorio, R. Hovsapian, J. C. Ordonez, Dynamic analysis of concentrated solar supercritical CO_2-based power generation closed-loop cycle, Appl. Therm. Eng. 93 (2016) 920–934.

[13] A. McMahan, S. Klein, D. Reindl, A finite-time thermodynamic framework for optimizing solar-thermal power plants, J. Sol. Energ. Eng. 129 (2007) 355–362.

[14] V. Zare, M. Hasanzadeh, Energy and exergy analysis of a closed brayton cycle-based combined cycle for solar power tower plants, Ener. Conv. Manage. 128 (2016) 227–237.

[15] M. Atif, F. Al-Sulaiman, Energy and exergy analyses of solar tower power plant driven supercritial carbon dioxide recompression cycles for six different locations, Renew. Sust. Ener. Rev. 68 (2017) 153–167.

[16] G. Barigozzi, G. Bonetti, G. Franchini, A. Perdichizzi, S. Ravelli, Thermal performance prediction of a solar hybrid gas turbine, Sol. Energy 86 (2012) 2116–2127.

[17] G. Barigozzi, A. Perdichizzi, C. Gritti, I. Guaiatelli, Techno-economic analysis of gas turbine inlet air cooling for combined cycle power plant for different climatic conditions, Appl. Therm. Eng. 82 (2015) 57–67.

[18] D. Milani, M. Tri Luu, R. McNaughton, A. Abbas, A comparative study of solar heliostat assisted supercritical CO_2 recompression Brayton cycles: Dynamic modelling and control strategies, J. of Supercritical Fluids 120 (2017) 113–124.

[19] C. Kalathakis, N. Aretakis, I. Roumeliotis, A. Alexiou, K. Mathioudakis, Concentrated solar power components toolbox in an object oriented environment, Sim. Model. Prac. Theo. 70 (2017) 21–35.

[20] B. Iverson, T. Conboy, J. Pasch, A. Kruizenga, Supercritical CO_2 Brayton cycles for solar-thermal energy, Appl. Energ. 111 (2013) 957–970.

[21] F. Al-Sulaiman, M. Atif, Performance comparison of different supercritical carbon dioxide Brayton cycles integrated with a solar power tower, Energy 82 (2015) 61–71.

[22] M. T. Luu, D. Milani, M. R., A. Abbas, Dynamic modelling and start-up operation of a solar-assisted recompression supercritical CO_2 Brayton power cycle, Appl. Ener. 199 (2017) 247–263.

[23] R. Vasquez Padilla, Y. Soo Too, R. Benito, R. McNaughton, W. Stein, Thermodynamic feasibility of alternative supercritical CO_2 Brayton cycles integrated with an ejector, Appl. Ener. 169 (2016) 49–62.

[24] Y. Ahn, S. J. Bae, M. Kim, S. Cho, S. Baik, J. E. Cha, Review of supercritical CO_2 power cycle technology and current status of research and development, Nucl. Eng. Technol. 47 (2015) 647–661.

[25] J. Muñoz-Antón, C. Rubbia, A. Rovira, J. M. Martínez-Val, Performance study of solar power plants with CO_2 as working fluid. A promising design window, Energ. Conv. Manage. 92 (2015) 36–46.

[26] Y. Muto, T. Ishizuka, M. Aritomi, N. Watanabe, Comparison of supercritical co_2 gas turbine cycle and Brayton co_2 gas turbine cycle for solar thermal power plants, The 4th International Symposium - Supercritical CO_2 Power Cycles, Pittsburgh, Pennsylvania, 2014.

[27] M. A. Reyes-Belmonte, A. Sebastián, M. Romero, J. González-Aguilar, Optimization of a recompression supercritical carbon dioxide cycle for an innovative central receiver solar power plant, Energy 112 (2016) 17–27.

[28] S. Sánchez-Orgaz, A. Medina, A. Calvo Hernández, Recuperative solar-driven multi-step gas turbine power plants, Energ. Convers. Manage. 67 (2013) 171–178.

[29] D. Olivenza-León, A. Medina, A. Calvo Hernández, Thermodynamic modeling of a hybrid solar gas-turbine power plant, Energ. Convers. Manage. 93 (2015) 435–447.

[30] M. J. Santos, R. P. Merchán, A. Medina, A. Calvo Hernández, Seasonal thermodynamic prediction of the performance of a hybrid solar gas-turbine power plant, Energ. Convers. Manage. 115 (2016) 89–102.

[31] M. Quero, R. Korzynietz, M. Ebert, A. A. Jiménez, A. del Río, J. A. Brioso, Solugas - operation experience of the first solar hybrid gas turbine system at MW scale, Energ. Proc. 49 (2014) 1820–1830.

[32] J. Heywood, Internal Combustion Engine Fundamentals, McGraw-Hill, 1988.

[33] J. Duffie, W. Beckman, Solar Engineering of Thermal Processes, John Wiley and Sons, Hoboken, New Jersey, 2006.

[34] V. Siva Reddy, S. C. Kaushik, S. K. Tyagi, Exergetic analysis and economic evaluation of central tower receiver solar thermal power plant, Int. J. Ener. Res. 38 (2014) 1288–1303. doi:10.1002/er.3138.

[35] Solar, Turbines, Caterpillar. [link].
URL `https://mysolar.cat.com/cda/files/126873/7/dsm50pg.pdf`

[36] Y. Najjar, M. Zaamout, Comparative performance of closed cycle gas turbine engine with heat recovery using different gases, Heat Recovery Syst. & CHP 12 (1992) 489–495.

[37] E. W. Lemmon, M. L. Huber, M. O. McLinden, NIST Standard Reference Database 23: Reference fluid thermodynamic and transport properties-REFPROP, version 9.1, National Institute of Standards and Technology, Standard Reference Data Program, Gaithersburg (2013).

[38] H. C. No, J. H. Kim, H. M. Kim, A review of helium gas turbine technology for high temperature gas-cooled reactors, Nucl. Eng. Technol. 39 (2007) 21.

[39] C. F. McDonald, Helium turbomachinery operating experience from gas turbine power plants and test facilities, App. Therm. Eng. 44 (2012) 108–142.

[40] F. Crespi, G. Gavagnin, D. Sánchez, G. S. Martínez, Supercritical carbon dioxide cycles for power generation, Appl. Ener. 195 (2017) 152–183.

[41] L. Coco-Enríquez, J. Muñoz Antón, J. M. Martínez-Val, New text comparison between CO_2 and other supercritical working fluids (ethane, Xe, CH_4 and N_2) in line-focusing solar power plants coupled to supercritical Brayton power cycles, Int. J. Hydrogen Ener. 42 (2017) 17611–17631.

[42] R. Chacartegui, J. Muñoz de Escalona, D. Sánchez, B. Monje, T. Sánchez, Alternative cycles based on carbon dioxide for central receiver solar power, Appl. Thermal Eng. 31 (2011) 872–879.